Miniaturization of Rat-Race Coupler With Dual-Band Arbitrary Power Divisions Based on Stepped-Impedance Double-Sided Parallel-Strip Line

Lin-Sheng Wu, *Member, IEEE*, Junfa Mao, *Fellow, IEEE*, and Wen-Yan Yin, *Senior Member, IEEE*

***Abstract*— Generalized equations are presented for the design of a rat-race coupler with a phase inverter and an arbitrary power division, where its four arms are built by symmetric reciprocal lossless two-port networks. According to these equations, uniform- and stepped-impedance rat-race couplers are analyzed and synthesized with dual-band arbitrary power divisions. The relationships between the geometries and the design specifications of proposed dual-band rat-race couplers are completely determined. Under such circumstances, the most compact configuration of the stepped-impedance rat-race coupler is achieved when the maximum allowable impedance ratio is applied for all its arms. Several prototypes are realized with double-sided parallel-strip lines (DSPSLs) and DSPSL phase inverters. As the stepped-impedance arms are not limited to simulate 90° sections and the phase inverters are implemented into our proposed dual-band couplers, the component circumferences are reduced significantly by 65%–70%, in comparison with their conventional 540° counterpart. Their good performances are demonstrated by the simulated and measured results.**

***Index Terms*— Arbitrary power division, double-sided parallel-strip line (DSPSL), dual band, miniaturization, rat-race coupler, stepped impedance.**

I. Introduction

A RAT-RACE coupler is one of the most essential passive couplers for RF and microwave systems and packages, which has been applied for the development of various mixers, amplifiers, antenna arrays, and so on. Usually, rat-race couplers are designed with equal power division. However, when they are used in some feed networks to replace power dividers, their unequal power division may also be desired. By controlling the characteristic admittances of its sections, a 540° rat-race coupler can have an arbitrary power division ratio [1], [2]. Stepped-impedance sections are utilized instead of uniform-impedance ones, which is good for the size reduction of the rat-race coupler with an arbitrary power division [3]. Its miniaturization can also be obtained by inserting a phase inverter into a 90° section to replace the 270° arm. Some generalized design methods are proposed in [4] and [5] for the wideband rat-race coupler with an ideal phase inverter and an arbitrary power division ratio.

With the rapid development of dual-band and multiband communication systems, dual-band and multiband RF components have drawn much attention recently, because of their small sizes and collaborative design concepts especially for system on package (SoP). Currently, the dual-band operation is one of the focuses of research in the realization of rat-race couplers. For example, the dual-band rat-race couplers are constructed by loading shorted or open stubs [6]–[8]. An impedance transformer, including two open stubs and a stepped-impedance line, has been utilized to replace the six 90° sections in a conventional rat-race coupler, within two specific bands simultaneously [9]. It has also been used to design a compact dual-band rat-race coupler with a phase inverter [10], in the form of double-sided parallel-strip line (DSPSL) [11]. But in [12], a dual-band rat-race coupler is built up by loading some stepped-impedance open stubs. With the uniform-impedance C-sections [13] and stepped-impedance ones [14], a phase shift of 90° and 270° can be synthesized at the first and second frequencies of the dual-band rat-race couplers, respectively.

The composite right or left-handed (CRLH) technique is another efficient choice for the design of a dual-band rat-race coupler. In [15], a dual-band coupler is realized by six CRLH transmission lines instead of normal 90° sections. In [16], different lumped-element CRLH sections are used to substitute for the 90° and 270° sections. A compact CRLH dual-band rat-race coupler is designed in low-temperature co-fired ceramic [17]. The complementary split-ring resonators are also used to build up a dual-band rat-race coupler [18]. Further, the CRLH half-mode substrate integrated waveguide is also utilized in [19]. The lumped elements and complicated

Manuscript received January 9, 2012; revised March 28, 2012; accepted July 27, 2012. Date of publication October 2, 2012; date of current version December 3, 2012. This work was supported in part by the National Basic Research Program of China under Grant 2009CB320204, the National Natural Science Foundation of China under Grant 61001014, the China Post-Doctoral Science Foundation under Grants 20100470702 and 201104268, and the Shanghai Post-Doctoral Scientific Program under Grant 11R21414000. Recommended for publication by Associate Editor A. Maffucci upon evaluation of reviewers' comments.

L.-S. Wu and J. Mao are with the Key Laboratory of Ministry of Education for Research of Design and Electromagnetic Compatibility of High Speed Electronic Systems, Shanghai Jiao Tong University, Shanghai 200240, China (e-mail: wallish@sjtu.edu.cn; jfmao@sjtu.edu.cn).

W.-Y. Yin is with the Key Laboratory of Ministry of Education for Research of Design and Electromagnetic Compatibility of High Speed Electronic Systems, Shanghai Jiao Tong University, Shanghai 200240, China, and also with the Center for Optical and EM Research, State Key Laboratory of MOI, Zhejiang University, Hangzhou 310058, China (e-mail: wyyin@sjtu.edu.cn).

Color versions of one or more of the figures in this paper are available online at http://ieeexplore.ieee.org.

Digital Object Identifier 10.1109/TCPMT.2012.2211597

unit cells in CRLH rat-race couplers, however, may lead to large losses.

According to the above approaches, many compact dual-band rat-race couplers with equal power divisions have been developed in the past several years. On the other hand, we would like to indicate the requirement of different individual power division ratios for some dual-band rat-race couplers, which will provide flexible and collaborative applications for SoP. Only few works, however, have been reported on the dual-band arbitrary power-division rat-race coupler until now.

As demonstrated in [20] and [21], the stub-loaded stepped-impedance unit and C-section structure have been successfully utilized for the construction of compact dual-band rat-race couplers with arbitrary power divisions, in which detailed design concerns are discussed and critical equations and curves are provided. However, both the stub-loaded and the C-section rat-race couplers, with equal or arbitrary power divisions, are started from the conventional prototype combined with 90° and 270° arms. Their configurations are still large for low operating frequencies under these circumstances. In addition, their bandwidths with small relative phase deviations are also limited. In [22], we proposed a new type of the DSPSL dual-band rat-race coupler with a phase inverter for the arbitrary power-division case, where a pair of arms is replaced with stepped-impedance sections for miniaturization.

In this paper, the design approach is extended and the coupler configuration is further miniaturized. At first, a set of generalized equations are derived for the rat-race coupler with a phase inverter and an arbitrary power division, where its four arms are represented by symmetric reciprocal lossless two-port networks. Then, the relationships between the geometries and design specifications of uniform-impedance dual-band rat-race couples are studied. When we apply the stepped-impedance technique for the design of a pair of arms, it is found that the ratio of size reduction reaches the upper limit as the maximum allowable impedance ratio is adopted. When all the arms are realized by stepped-impedance sections with the maximum impedance ratio, the most compact case is obtained. Because both electrical lengths and characteristic impedances of the sections are synthesized with more freedoms, significant size reductions in the coupler geometry have been achieved, as demonstrated by both simulated and measured results of several typical DSPSL coupler prototypes.

II. Arbitrary Power-Division Rat-Race Coupler With Generalized Symmetric Two-Port Networks

Fig. 1(a) shows the schematic of a generalized rat-race coupler with an ideal phase inverter, where each arm is represented by a symmetric reciprocal lossless two-port network. The opposite arms are with the same two-port networks. The frequency response of the coupler with an ideal phase inverter, which is located on the symmetric plane of the two-port network $\mathbf{Y}^B$ between ports 2 and 3, is the same as that with the configuration shown in Fig. 1(a). The equivalent circuit models of the coupler for even- and odd-mode excitations are shown in Fig. 1(b) and (c), respectively.

It is seen that the odd-mode circuit model can be obtained from the even-mode one by exchanging the left and the right

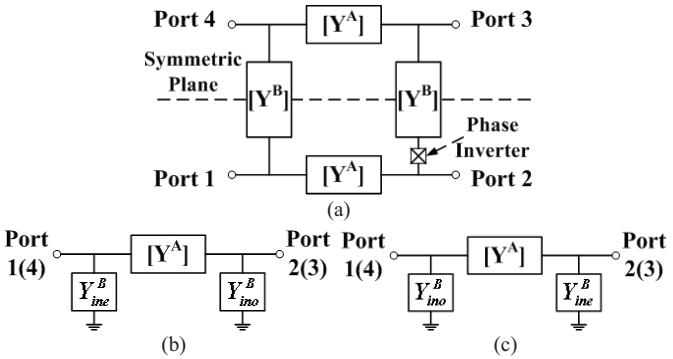

Fig. 1. Rat-race coupler with an ideal phase inverter, where each arm is realized by a symmetric two-port network. (a) Its schematic. (b) Its even-mode circuit model. (c) Odd-mode circuit model.

sides. Thus, S-parameters of the rat-race coupler are expressed as

$$S_{11} = \frac{S^e_{11} + S^o_{11}}{2} = \frac{S^e_{11} + S^e_{22}}{2} \tag{1a}$$

$$S_{21} = \frac{S^e_{21} + S^o_{21}}{2} = S^e_{21} \tag{1b}$$

$$S_{41} = \frac{S^e_{11} - S^o_{11}}{2} = \frac{S^e_{11} - S^e_{22}}{2} \tag{1c}$$

$$S_{23} = \frac{S^e_{22} - S^o_{22}}{2} = \frac{S^e_{22} - S^e_{11}}{2} = -S_{41} \tag{1d}$$

$$S_{33} = \frac{S^e_{22} + S^o_{22}}{2} = \frac{S^e_{11} + S^e_{22}}{2} = S_{11} \tag{1e}$$

$$S_{43} = S_{21} \tag{1f}$$

$$S_{31} = \frac{S^e_{21} - S^o_{21}}{2} = 0 \tag{1g}$$

where the superscripts "e" and "o" correspond to the even- and odd-mode models, respectively, and

$$\begin{bmatrix} S^e_{11} & S^e_{21} \\ S^e_{21} & S^e_{22} \end{bmatrix} = \begin{bmatrix} S^o_{22} & S^o_{21} \\ S^o_{21} & S^o_{11} \end{bmatrix} = \begin{bmatrix} \frac{a+b-c-d}{a+b+c+d} & \frac{2}{a+b+c+d} \\ \frac{2}{a+b+c+d} & \frac{b+d-a-c}{a+b+c+d} \end{bmatrix} \tag{2a}$$

$$a = -\frac{Y^A_{11} + Y^B_{\text{ino}}}{Y^A_{21}} \tag{2b}$$

$$b = -\frac{Y_p}{Y^A_{21}} \tag{2c}$$

$$c = -\frac{\left(Y^A_{11}\right)^2 - \left(Y^A_{21}\right)^2 + Y^A_{11}Y^B_{\text{ine}} + Y^A_{11}Y^B_{\text{ino}} + Y^B_{\text{ine}}Y^B_{\text{ino}}}{Y^A_{21}Y_p} \tag{2d}$$

$$d = -\frac{Y^A_{11} + Y^B_{\text{ine}}}{Y^A_{21}} \tag{2e}$$

where Y_p is the admittance of four ports and is usually set to 1/50 Ω^{-1}. As shown in Fig. 1, Y^B_{ine} and Y^B_{ino} are the even- and odd-mode input admittances of the two-port network $\mathbf{Y}^B$ and are given by

$$Y^B_{ine} = Y^B_{11} + Y^B_{21} \tag{3a}$$

$$Y^B_{ino} = Y^B_{11} - Y^B_{21}. \tag{3b}$$

From (1g), it is found that the perfect isolation condition, with the ideal phase inverter used, is always satisfied. According to (1a), (1e), (2a), (2c), and (2d), the perfect matching

condition is satisfied only when $b = c$, i.e.,

$$\left(Y_{21}^{A}\right)^2 + \left(Y_{21}^{B}\right)^2 + Y_p^2 = \left(Y_{11}^{A} + Y_{11}^{B}\right)^2. \tag{4a}$$

Since both $\mathbf{Y}^A$ and $\mathbf{Y}^B$ are lossless networks, (4a) can be rewritten as

$$\left[\mathrm{Im}\left(\mathrm{Y}_{11}^{\mathrm{A}}\right) + \mathrm{Im}\left(\mathrm{Y}_{11}^{\mathrm{B}}\right)\right]^2 + Y_p^2 = \mathrm{Im}^2\left(Y_{21}^{A}\right) + \mathrm{Im}^2\left(Y_{21}^{B}\right) \tag{4b}$$

where Im(·) represents the imaginary part.

From (1)–(3), the amplitude ratio between two outputs is derived as

$$\frac{S_{21}}{S_{41}} = \frac{S_{43}}{-S_{23}} = \frac{2}{a-d} = \frac{Y_{21}^{A}}{Y_{21}^{B}}. \tag{5a}$$

Equation (5a) can also be written as

$$\frac{S_{21}}{S_{41}} = \frac{S_{43}}{-S_{23}} = \frac{\mathrm{Im}\left(Y_{21}^{A}\right)}{\mathrm{Im}\left(Y_{21}^{B}\right)} = R_p \tag{5b}$$

where R_p is defined as the amplitude ratio of S_{21} to S_{41}.

When both (4b) and (5b) are satisfied at a specific frequency, one rat-race coupler can be determined with a certain power division. If the equations are ensured at two or more specific frequencies individually, a dual-band or multiband coupler is then obtained.

III. Uniform-Impedance Rat-Race Coupler With Dual-Band Arbitrary Power Divisions

Fig. 2 shows the schematic of a rat-race coupler with an ideal phase inverter. Its four arms are all implemented with uniform-impedance transmission lines. In this case, the Y-parameters of four arms are given as

$$\mathrm{Im}\left(Y_{11}^{A}\right) = -Y_1 \cot\theta_1 \tag{6a}$$

$$\mathrm{Im}\left(Y_{21}^{A}\right) = Y_1 \csc\theta_1 \tag{6b}$$

$$\mathrm{Im}\left(Y_{11}^{B}\right) = -Y_2 \cot\theta_2 \tag{6c}$$

$$\mathrm{Im}\left(Y_{21}^{B}\right) = Y_2 \csc\theta_2. \tag{6d}$$

Then, (4b) and (5b) are in the forms of

$$Y_1^2 + Y_2^2 - 2Y_1Y_2\cot\theta_1\cot\theta_2 = Y_p^2 \tag{7a}$$

$$\frac{S_{21}}{S_{41}} = \frac{S_{43}}{-S_{23}} = \frac{Y_1\csc\theta_1}{Y_2\csc\theta_2} = R_p. \tag{7b}$$

The two equations are identical to those derived in [4].

When both θ_1 and θ_2 are limited to 90°, Y_1 and Y_2 can be uniquely determined by

$$Y_1 = \frac{Y_p}{\sqrt{1 + 1\Big/R_p^2}} \tag{8a}$$

$$Y_2 = \frac{Y_p}{\sqrt{1 + R_p^2}}. \tag{8b}$$

There is no design freedom for other specific considerations. Thus, if one dual-band rat-race coupler is demanded, the electrical lengths θ_1 and θ_2 should not be preset to 90°.

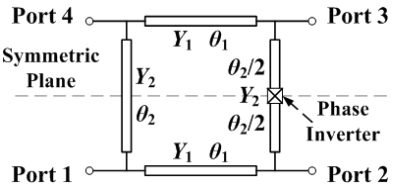

Fig. 2. Schematic of a uniform-impedance rat-race coupler with an ideal phase inverter.

For the uniform-impedance dual-band coupler, the following four equations should be satisfied simultaneously, i.e.,

$$\frac{Y_2}{Y_1} = \frac{\sin\theta_2}{R_{p1}\sin\theta_1} \tag{9a}$$

$$\frac{Y_2}{Y_1} = \frac{\sin n\theta_2}{R_{p2}\sin n\theta_1} \tag{9b}$$

$$\cot\theta_1\cot\theta_2 = \frac{Y_1^2 + Y_2^2 - Y_p^2}{2Y_1Y_2} \tag{9c}$$

$$\cot n\theta_1\cot n\theta_2 = \frac{Y_1^2 + Y_2^2 - Y_p^2}{2Y_1Y_2} \tag{9d}$$

where n is the ratio of the second operating frequency f_2 to the first operating frequency f_1, θ_1 and θ_2 are the electrical lengths at f_1, and R_{p1} and R_{p2} are the amplitude ratios between two outputs at f_1 and f_2, respectively. For the given n, R_{p1}, and R_{p2}, θ_1 and θ_2 are solved by

$$\frac{\sin\theta_2}{\sin\theta_1} = \frac{R_{p1}}{R_{p2}}\frac{\sin n\theta_2}{\sin n\theta_1} \tag{10a}$$

$$\cot\theta_1\cot\theta_2 = \cot n\theta_1\cot n\theta_2. \tag{10b}$$

The normalized circumference at f_1 of the uniform-impedance dual-band rat-race coupler with arbitrary power divisions is

$$\phi\left(n,\ R_{p1},\ R_{p2}\right) = 2\left(\theta_1 + \theta_2\right). \tag{11}$$

Then, Y_1 and Y_2 are calculated by

$$Y_1 = \frac{Y_p}{\sqrt{1 + \frac{1}{R_{p1}^2}\frac{\sin^2\theta_2}{\sin^2\theta_1} - \frac{2}{R_{p1}}\frac{\cos\theta_1\cos\theta_2}{\sin^2\theta_1}}} \tag{12a}$$

$$Y_2 = \frac{Y_p}{\sqrt{1 + R_{p1}^2\frac{\sin^2\theta_1}{\sin^2\theta_2} - 2R_{p1}\frac{\cos\theta_1\cos\theta_2}{\sin^2\theta_2}}}. \tag{12b}$$

To synthesize a uniform-impedance rat-race coupler with dual-band arbitrary power divisions, the relationships between its geometries and design specifications are obtained from (10)–(12), as plotted in Fig. 3(a)–(f).

Fig. 3(a) shows that the circumference decreases with decreasing $|\mathrm{dB}(R_{p2}) - \mathrm{dB}(R_{p1})|$ and it reaches its minimum when $R_{p1} = R_{p2}$. If one special value is given for n, the minimum circumference is also determined. In Fig. 3(b), θ_1 increases with decreasing R_{p1} and increasing R_{p2}, but θ_2 increases with increasing R_{p1} and decreasing R_{p2}. When $R_{p1} = R_{p2}$, $\theta_1 = \theta_2$. In Fig. 3(c), when $n = 2$, Y_1^{-1} decreases whereas Y_2^{-1} increases with increasing R_{p1} and R_{p2}. When $R_{p1} = R_{p2} = 0$ dB, we have $Y_1 = Y_2$.

Fig. 3(d) shows that, with $R_{p1} = 1$, the minimum value of circumference decreases when the frequency ratio n increases.

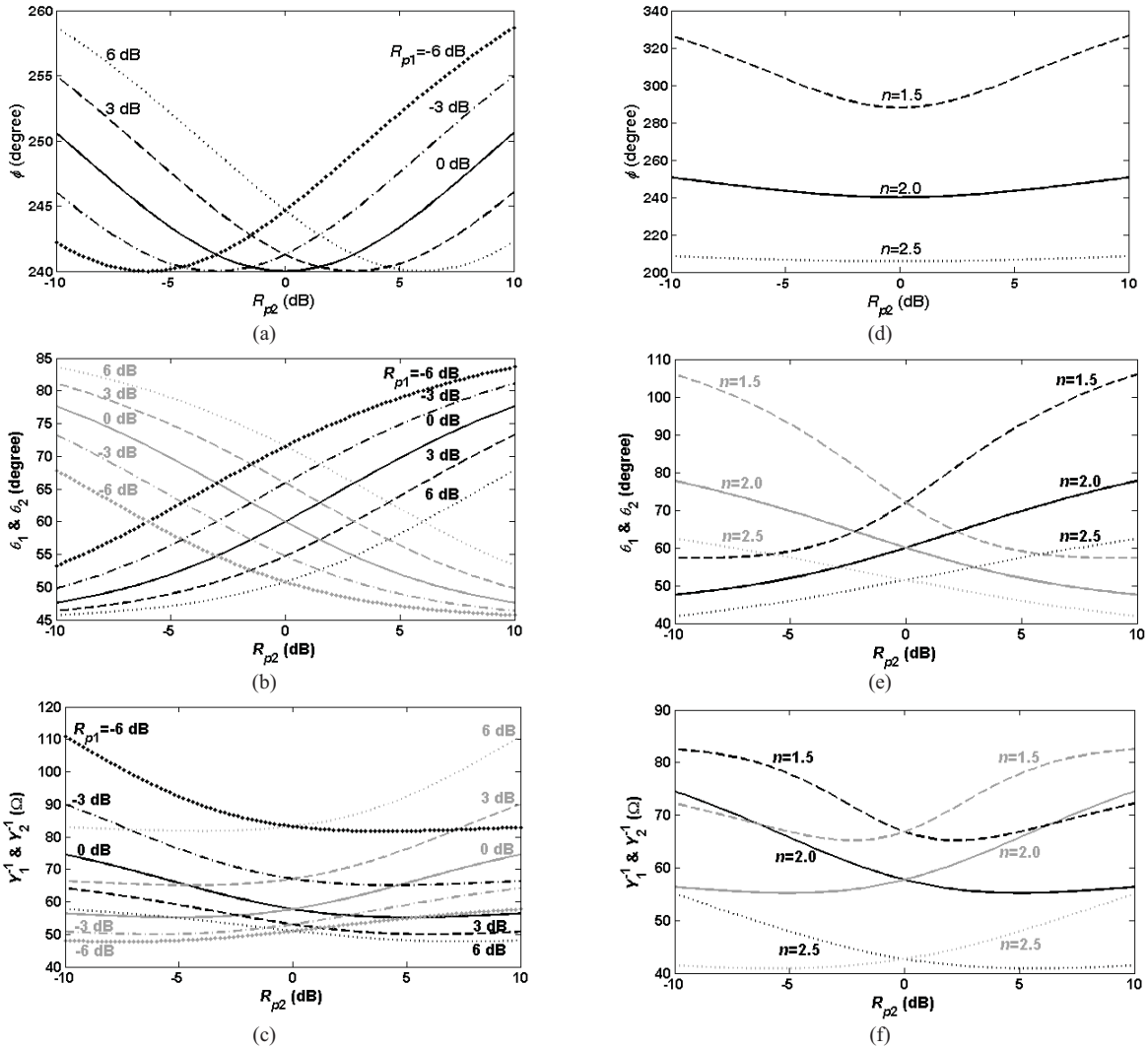

Fig. 3. Relationships between geometries and design specifications of the uniform-impedance rat-race coupler with dual-band arbitrary power divisions. (a)–(c) For different R_{p1} and R_{p2} with $n = 2$. (d)–(f) For different n and R_{p2} with $R_{p1} = 1$ (0 dB). (a) Circumferences. (b) θ_1 (black lines) and θ_2 (gray lines). (c) Y_1^{-1} (black lines) and Y_2^{-1} (gray lines). (d) Circumferences. (e) θ_1 (black lines) and θ_2 (gray lines). (f) Y_1^{-1} (black lines) and Y_2^{-1} (gray lines).

Correspondingly, the variation range of circumference, with different values of R_{p2} chosen, is reduced significantly. Fig. 3(e) and (f) shows that θ_1, θ_2, Y_1^{-1}, and Y_2^{-1} all decrease with increasing n. When n is relatively small, both Y_1^{-1} and Y_2^{-1} at first decrease and then increase with R_{p2}.

All cases plotted in Fig. 3(a)–(f) can be easily realized, as the synthesized characteristic impedances are always within the range of 40–120 Ω. At the same time, the synthesized electrical lengths are neither too small nor too large. So, with a uniform-impedance rat-race coupler, it is quite flexible to get the function of dual-band arbitrary power divisions.

IV. Dual-Band Arbitrary Power-Division Rat-Race Coupler With a Pair of Stepped-Impedance Arms

According to (10)–(12), it can be found that all the geometric parameters of the uniform-impedance rat-race coupler can be determined by the design specifications n, R_{p1}, and R_{p2}. No more design freedom is provided for its miniaturization. To make the configuration more compact, some stepped-impedance sections, as shown in Fig. 4, are introduced to replace a pair of uniform-impedance arms in Fig. 2.

In Fig. 4(a), the arms between Ports 1(4) and 2(3) are with the stepped-impedance sections and

$$\mathrm{Im}\left(Y_{11}^{A}\right) = \frac{Y_{1A}}{2}\left[\frac{Y_{1B}\tan\theta_{1B} + 2Y_{1A}\tan\left(\theta_{1A}/2\right)}{2Y_{1A} - Y_{1B}\tan\theta_{1B}\tan\left(\theta_{1A}/2\right)} - \cot\frac{\theta_{1A}}{2}\right] \tag{13a}$$

$$\mathrm{Im}\left(Y_{21}^{A}\right) = \frac{Y_{1A}}{2}\left[\frac{Y_{1B}\tan\theta_{1B} + 2Y_{1A}\tan\left(\theta_{1A}/2\right)}{2Y_{1A} - Y_{1B}\tan\theta_{1B}\tan\left(\theta_{1A}/2\right)} + \cot\frac{\theta_{1A}}{2}\right] \tag{13b}$$

$$\mathrm{Im}\left(Y_{11}^{B}\right) = -Y_2\cot\theta_2 \tag{13c}$$

$$\mathrm{Im}\left(Y_{21}^{B}\right) = Y_2\csc\theta_2. \tag{13d}$$

By substituting (13) into (4b) and (5b), a set of design equations is obtained and it should be enforced at both of the two operating frequencies f_1 and f_2. If the characteristic admittance Y_{1B} and the electrical length θ_{1B} are preset, θ_{1A}, θ_2, Y_{1A}, and Y_2 can be solved for the given design specifications of n, R_{p1}, and R_{p2}. The circumference of the rat race is calculated by

$$\phi\left(n,\ R_{p1},\ R_{p2}\right) = 2\left(\theta_{1A} + \theta_{1B} + \theta_2\right). \tag{14}$$

For the schematic in Fig. 4(b), we have

$$\mathrm{Im}\left(Y_{11}^{A}\right) = -Y_1 \cot\theta_1 \tag{15a}$$

$$\mathrm{Im}\left(Y_{21}^{A}\right) = Y_1 \csc\theta_1 \tag{15b}$$

$$\mathrm{Im}\left(Y_{11}^{B}\right) = \frac{Y_{2A}}{2}\left[\frac{Y_{2B}\tan\theta_{2B} + 2Y_{2A}\tan\left(\theta_{2A}/2\right)}{2Y_{2A} - Y_{2B}\tan\theta_{2B}\tan\left(\theta_{2A}/2\right)} - \cot\frac{\theta_{2A}}{2}\right] \tag{15c}$$

$$\mathrm{Im}\left(Y_{21}^{B}\right) = \frac{Y_{2A}}{2}\left[\frac{Y_{2B}\tan\theta_{2B} + 2Y_{2A}\tan\left(\theta_{2A}/2\right)}{2Y_{2A} - Y_{2B}\tan\theta_{2B}\tan\left(\theta_{2A}/2\right)} + \cot\frac{\theta_{2A}}{2}\right]. \tag{15d}$$

Also substitute (15) into (4b) and (5b). The design equations are easily obtained and the circumference can be calculated by

$$\phi\left(n,\ R_{p1},\ R_{p2}\right) = 2\left(\theta_1 + \theta_{2A} + \theta_{2B}\right). \tag{16}$$

Therefore, for the dual-band arbitrary power-division rat-race couplers, with a pair of stepped-impedance arms shown in Fig. 4, all the values of Y_{1A}, Y_2, θ_{1A}, and θ_2 (Y_1, Y_{2A}, θ_1, and θ_{2A}) can be controlled by Y_{1B} and θ_{1B} (Y_{2B} and θ_{2B}) and then the component miniaturization is further achieved.

The design curves of the rat-race couplers in Fig. 4(a) and (b) are plotted in Figs. 5 and 6, respectively, where the design specifications are given by $n = 2$, $R_{p1} = 1$ (0 dB), and $R_{p2} = 2.0$ (6 dB). The realizable characteristic impedance is set between 30 and 210 Ω here. One can utilize the curves to quickly design a specific coupler with such two configurations. All the synthesized geometric parameters start from their corresponding values of the uniform-impedance schematic, that is, $\theta_{1B} = 0$ or $\theta_{2B} = 0$.

Fig. 5 shows that the circumference of the coupler always decreases with an increase of θ_{1B} when Y_{1B} is fixed. The circumference reaches its minimum when the upper or lower limit of Y_{1A} is adopted. As Y_{1B} is set to 1/30, 1/40, and 1/50 Ω^{-1}, the minimum circumference is obtained with $Y_{1A} =$ 1/210 Ω^{-1}. As Y_{1B} is set to 1/60, 1/70, 1/80, 1/100, 1/130, 1/170, and 1/210 Ω^{-1}, the minimum circumference is obtained with $Y_{1A} =$ 1/30 Ω^{-1}. It indicates that a large impedance ratio is preferred for the stepped-impedance arms. The most compact design is achieved under the design specifications when $Y_{1A} =$ 1/30 Ω^{-1} and $Y_{1B} =$ 1/210 Ω^{-1}, corresponding to the maximum allowable impedance ratio of 7.

A similar conclusion can be drawn from Fig. 6. It is observed that the synthesized Y_1 and θ_1 change with Y_{2B} and θ_{2B} slightly, while the design values of Y_{2A} and θ_{2A} are significantly influenced by Y_{2B} and θ_{2B}. As Y_{2B} is set to 1/30, 1/40, 1/50, and 1/60 Ω^{-1}, the minimum circumference is obtained with $Y_{2A} =$ 1/210 Ω^{-1}. As Y_{2B} is set to 1/70, 1/80, 1/100, 1/130, 1/170, and 1/210 Ω^{-1}, the minimum circumference is obtained with $Y_{2A} =$ 1/30 Ω^{-1}. For the schematic shown in Fig. 4(b), the most compact configuration is obtained when $Y_{2A} =$ 1/30 Ω^{-1} and $Y_{2B} =$ 1/210 Ω^{-1}, which means the maximum impedance ratio of 7 is still desired.

Although both stepped-impedance schematics in Fig. 4(a) and (b) can be utilized to miniaturize the dual-band rat-race coupler with arbitrary power divisions, the largest size reductions obtained with them are different, when the coupler has unequal power divisions. The synthesized geometric parameters, with the three schematics shown in Figs. 2 and 4(a) and (b), are summarized in Table I for comparison, where the design specifications are given by

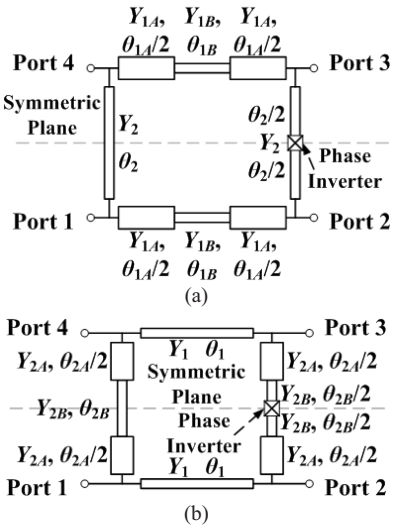

Fig. 4. Schematics of two dual-band arbitrary power-division rat-race couplers with a pair of stepped-impedance arms. (a) SI1 case. (b) SI2 case.

TABLE I
COMPARISON OF THE SYNTHESIZED PARAMETERS OF THE DUAL-BAND RAT-RACE COUPLERS WITH ARBITRARY POWER DIVISIONS BETWEEN DIFFERENT SCHEMATICS

	UI	SI1	SI2	LHLH	LHHL	HLLH	HLHL
Y_1^{-1}/Y_{1A}^{-1}	55.3	30.0	51.4	30.0	30.0	210	210
θ_1/θ_{1A}	71.6	57.2	64.7	55.8	57.7	13.3	13.4
Y_{1B}^{-1}	/	210	/	210	210	30.0	30.0
θ_{1B}	/	6.48	/	6.07	6.61	21.7	27.3
Y_2^{-1}/Y_{2A}^{-1}	67.7	110	30.0	30.0	210	30.0	210
θ_2/θ_{2A}	50.8	23.1	24.8	7.29	11.8	37.7	13.1
Y_{2B}^{-1}	/	/	210	210	30.0	210	30.0
θ_{2B}	/	/	9.82	10.5	3.75	9.33	24.1
ϕ	245	174	199	159	160	164	156
a_1	1.00	0.71	0.81	0.65	0.65	0.67	0.64
a_2	0.45	0.32	0.37	0.30	0.30	0.30	0.29

[1]The characteristic impedances are in Ω. The electrical lengths and circumferences are in degrees.
[2]The values of a_1 and a_2 are the ratios of the circumference to those of the UI schematic and the conventional 540° counterpart, respectively.
[3]The above two notes are also applied for Table III.

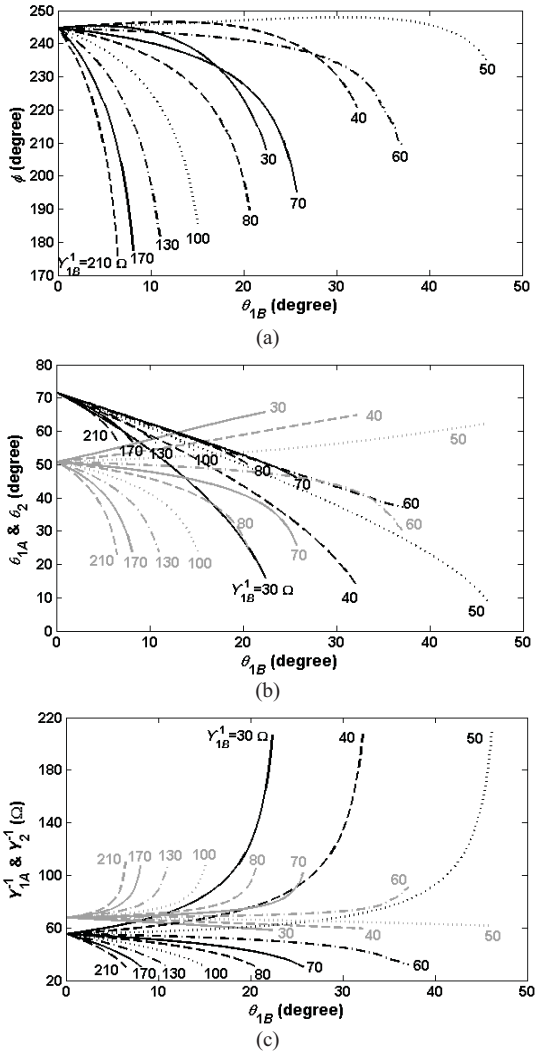

Fig. 5. Shown are synthesized Y_{1A}, Y_2, θ_{1A}, and θ_2 and the circumference for different values of Y_{1B} and θ_{1B} of the rat-race coupler in Fig. 4(a), where $n = 2$, $R_{p1} = 1$ (0 dB), and $R_{p2} = 2.0$ (6 dB). (a) Circumferences. (b) θ_{1A} (black lines) and θ_2 (gray lines). (c) Y_{1A}^{-1} (black lines) and Y_2^{-1} (gray lines).

$n = 2$, $R_{p1} = 1$ (0 dB), and $R_{p2} = 2.0$ (6 dB). "UI" represents the uniform-impedance schematic in Fig. 2, and "SI1" and "SI2" represent the minimum configurations with the stepped-impedance ones in Fig. 4(a) and (b), respectively. The circumferences of SI1 and SI2 cases are reduced by 71° and 46°, respectively, in comparison with their uniform-impedance counterpart. Under such design specifications, better miniaturization can be achieved when we apply the stepped-impedance technique for the arms handling with higher power. It is also noted that, as the stepped-impedance rat-race coupler in [22] is not designed with the maximum impedance ratio of 7, its circumference of 182° is 8° larger than the synthesized 174° of the SI1 case in Table I.

V. Dual-Band Arbitrary Power-Division Rat-Race Coupler With Four Stepped-Impedance Arms

To further miniaturize the dual-band rat-race coupler with arbitrary power-divisions, its four arms, as shown in Fig. 7, are

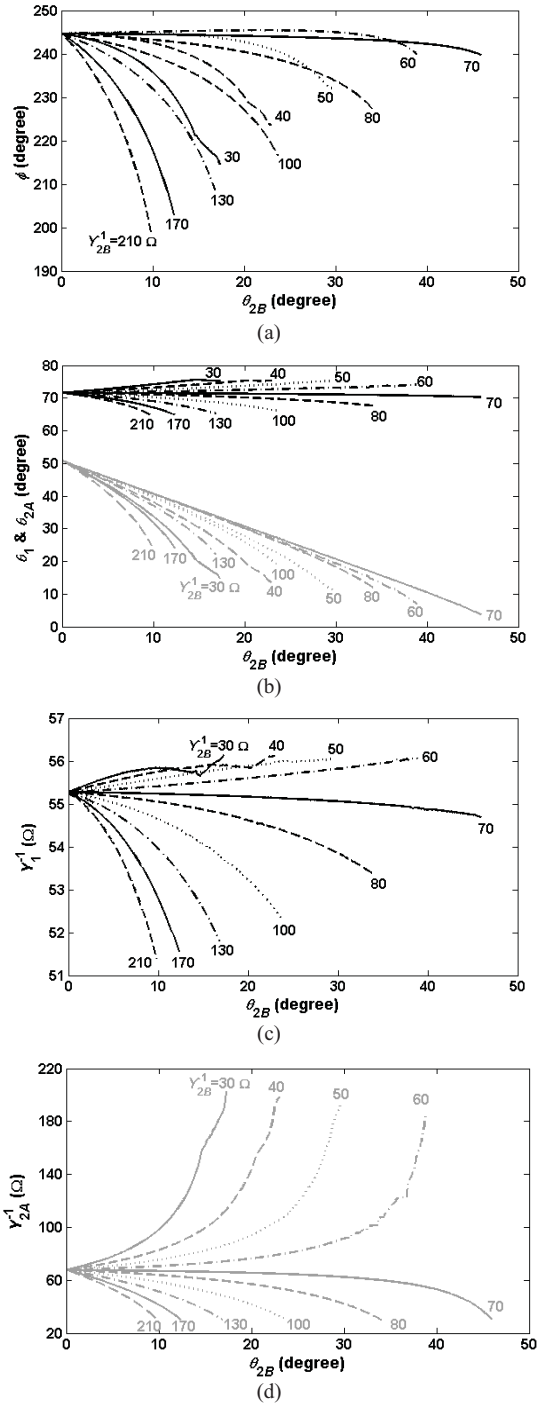

Fig. 6. Shown are synthesized Y_1, Y_{2A}, θ_1, and θ_{2A} and the circumference for different values of Y_{2B} and θ_{2B} of the rat-race coupler in Fig. 4(b), where $n = 2$, $R_{p1} = 1$ (0 dB), and $R_{p2} = 2.0$ (6 dB). (a) Circumferences. (b) θ_1 (black lines) and θ_{2A} (gray lines). (c) Y_1^{-1}. (d) Y_{2A}^{-1}.

all realized by using stepped-impedance sections. Therefore, we have

$$\mathrm{Im}\left(Y_{11}^{A}\right) = \frac{Y_{1A}}{2}\left[\frac{Y_{1B}\tan\theta_{1B} + 2Y_{1A}\tan\left(\theta_{1A}/2\right)}{2Y_{1A} - Y_{1B}\tan\theta_{1B}\tan\left(\theta_{1A}/2\right)} - \cot\frac{\theta_{1A}}{2}\right] \tag{17a}$$

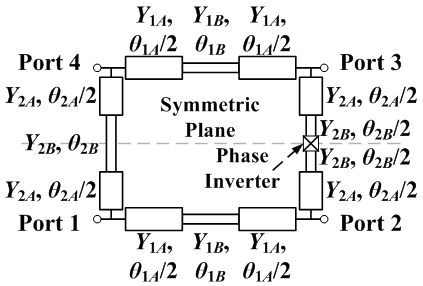

Fig. 7. Schematic of the stepped-impedance rat-race coupler.

$$\mathrm{Im}\left(Y_{21}^{A}\right) = \frac{Y_{1A}}{2}\left[\frac{Y_{1B}\tan\theta_{1B} + 2Y_{1A}\tan\left(\theta_{1A}/2\right)}{2Y_{1A} - Y_{1B}\tan\theta_{1B}\tan\left(\theta_{1A}/2\right)} + \cot\frac{\theta_{1A}}{2}\right] \tag{17b}$$

$$\mathrm{Im}\left(Y_{11}^{B}\right) = \frac{Y_{2A}}{2}\left[\frac{Y_{2B}\tan\theta_{2B} + 2Y_{2A}\tan\left(\theta_{2A}/2\right)}{2Y_{2A} - Y_{2B}\tan\theta_{2B}\tan\left(\theta_{2A}/2\right)} - \cot\frac{\theta_{2A}}{2}\right] \tag{17c}$$

$$\mathrm{Im}\left(Y_{21}^{B}\right) = \frac{Y_{2A}}{2}\left[\frac{Y_{2B}\tan\theta_{2B} + 2Y_{2A}\tan\left(\theta_{2A}/2\right)}{2Y_{2A} - Y_{2B}\tan\theta_{2B}\tan\left(\theta_{2A}/2\right)} + \cot\frac{\theta_{2A}}{2}\right]. \tag{17d}$$

The corresponding design equations, obtained by substituting (17) into (4b) and (5b), should be satisfied at both f_1 and f_2. Then, the coupler circumference is

$$\varphi\left(n,\ R_{p1},\ R_{p2}\right) = 2\left(\theta_{1A} + \theta_{1B} + \theta_{2A} + \theta_{2B}\right). \tag{18}$$

There are eight geometric parameters, Y_{1A}, Y_{1B}, Y_{2A}, Y_{2B}, θ_{1A}, θ_{1B}, θ_{2A}, and θ_{2B}, for the four design equations. In other words, four parameters can be properly selected to provide the most compact configuration of the rat-race coupler, which is quite important for packaging systems.

A detailed study has been carried out in the parameter space, still under the design specifications of $n = 2$, $R_{p1} = 1$ (0 dB), and $R_{p2} = 2.0$ (6 dB). It is found that the most compact configuration is achieved when both of the two pairs of stepped-impedance arms are with the maximum impedance ratio of 7, which is in consonance with the conclusion drawn in Section IV.

There are four cases with the maximum impedance ratio applied for the dual-band rat-race coupler with arbitrary power divisions.

1) LHLH case: $Y_{1A} = 1/30\ \Omega^{-1}$, $Y_{1B} = 1/210\ \Omega^{-1}$, $Y_{2A} = 1/30\ \Omega^{-1}$, and $Y_{2B} = 1/210\ \Omega^{-1}$.
2) LHHL case: $Y_{1A} = 1/30\ \Omega^{-1}$, $Y_{1B} = 1/210\ \Omega^{-1}$, $Y_{2A} = 1/210\ \Omega^{-1}$, and $Y_{2B} = 1/30\ \Omega^{-1}$.
3) HLLH case: $Y_{1A} = 1/210\ \Omega^{-1}$, $Y_{1B} = 1/30\ \Omega^{-1}$, $Y_{2A} = 1/30\ \Omega^{-1}$, and $Y_{2B} = 1/210\ \Omega^{-1}$.
4) HLHL case: $Y_{1A} = 1/210\ \Omega^{-1}$, $Y_{1B} = 1/30\ \Omega^{-1}$, $Y_{2A} = 1/210\ \Omega^{-1}$, and $Y_{2B} = 1/30\ \Omega^{-1}$.

The synthesized parameters and circumferences of the four cases are also summarized in Table I for comparison. Under the preset specifications, the four circumferences have close values. The HLHL case provides the most compact rat-race coupler, whose 156° circumference is 89° and 18° smaller than those of the UI and SI1 schematics. The second smallest circumference of 159° is obtained with the LHLH case. The HLHL case, however, is not preferred for this set of design specifications, because its bandwidth of the second band is very narrow, which will be shown in Section VI-B.

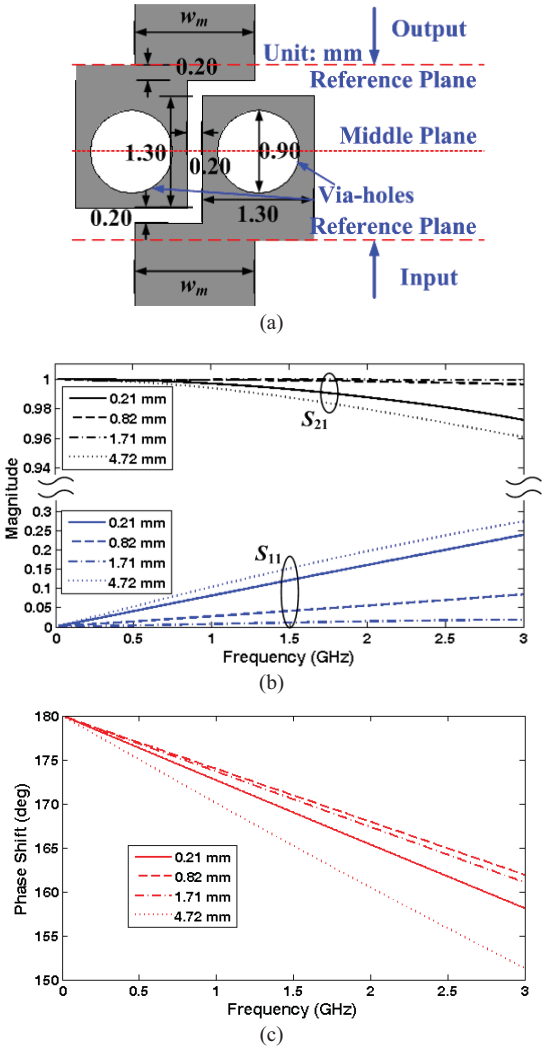

Fig. 8. DSPSL phase inverter. (a) Top view. (b) Magnitudes of simulated S_{11} and S_{21} with different w_m. (c) Phase shifts of S_{21} with different w_m.

Although the analyses in Sections IV and V are only carried out for the stepped-impedance topologies, the proposed design approach and equations, including (4b) and (5b), can also be applied for other miniaturized geometries, such as stub-loaded structures, C-sections, and other composite units.

VI. Realization and Discussion

A. DSPSL Phase Inverter

The coupler prototypes are implemented with the DSPSL structure in this paper, since the phase inverter can be easily realized by a DSPSL swap [11]. The F4B substrate is used, with its relative permittivity of 2.65 and its thickness

of 0.8 mm. The top view of the used phase inverter is shown in Fig. 8(a) with critical dimensions. Its bottom view can be obtained by reversing the top view along the middle plane. Here, w_m is determined by the required characteristic impedance Z_0 of the DSPSL lines that connect the phase inverter directly.

The simulated results of the phase inverter with different w_m are obtained by using the commercial electromagnetic simulator, Ansoft HFSS, and are plotted in Fig. 8(b) and (c). The values 0.21, 0.82, 1.71, and 4.72 mm of w_m correspond to the characteristic impedance Z_0 of 210, 110, 67.7, and 30 Ω, respectively. In the simulations of phase inverter, the two-port impedances are also set to Z_0.

It is found that both the magnitude of reflection coefficient and the phase shift are nearly linear to frequency. The phase inverter is approximately modeled by the combination of an ideal phase inverter and an additional transmission line, as shown in Fig. 9(a). Then, the reflection coefficient and phase shift can be approximated by

$$|S_{11}| = \left| \frac{j\left(Z_{pi}^2 - Z_0^2\right)\sin\omega t_{pi}}{2Z_{pi}Z_0\cos\omega t_{pi} + j\left(Z_{pi}^2 + Z_0^2\right)\sin\omega t_{pi}} \right| \approx \frac{\left|Z_{pi}^2 - Z_0^2\right| t_{pi}}{2Z_{pi}Z_0}\omega \quad (19a)$$

$$\angle S_{21} = arg\left[-\frac{2Z_{pi}Z_0}{2Z_{pi}Z_0\cos\omega t_{pi} + j\left(Z_{pi}^2 + Z_0^2\right)\sin\omega t_{pi}} \right] \approx \pi - \frac{\left(Z_{pi}^2 + Z_0^2\right) t_{pi}}{2Z_{pi}Z_0}\omega. \quad (19b)$$

From the simulated results, the equivalent characteristic impedance and time delay of the additional transmission line are estimated to be about $Z_{pi} = 88\ \Omega$ and $t_{pi} = 15.7$ ps, respectively. With these two parameters, the curves of $|S_{11}|$ and 180°-$\angle S_{21}$ are calculated for 1.5 GHz and plotted in Fig. 9(b) and (c), respectively. The simulated results at 1.5 GHz are also shown in the figures for comparison. Reasonable agreement is achieved between them and then the circuit model of the DSPSL phase inverter is demonstrated.

Our used phase inverter has a total physical length of $l_{pi} = 2.1$ mm. For a DSPSL line with a characteristic impedance of $Z_{pi} = 88\ \Omega$ and a length of l_{pi} on the same F4B substrate, it will have a time delay of $t_d = l_{pi} \times \text{sqrt}(\varepsilon_{re})/c_0$, where $\varepsilon_{re} = 2.20$ is the effective relative permittivity and c_0 is the wave velocity in vacuum. Then, we have $t_d = 10.4$ ps. In comparison with the combination of an ideal phase inverter and a DSPSL line of 2.1 mm, the used phase inverter will provide an additional time delay of $\Delta t = t_{pi} - t_d = 5.3$ ps. This leads to an additional phase shift of $\Delta\phi = f\Delta t \times 360°$ at a certain frequency f, which is equal to 1.7°, 2.6°, 3.4°, and 4.3° at the operating frequencies of 0.9, 1.35, 1.8, and 2.25 GHz, respectively.

It is numerically found that the DSPSL phase inverter has little influence on the Y-parameters of the transmission line inserted with it within the concerned frequency range, even when the characteristic impedance Z_0 of the transmission line is different from $Z_{pi} = 88\ \Omega$. The negative influence of the additional transmission line and the discontinuities caused by

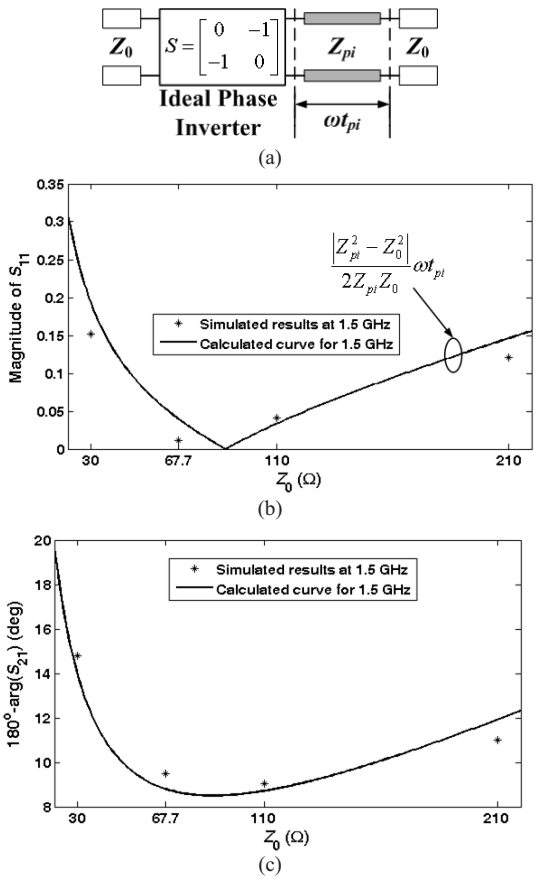

Fig. 9. Modeling of the DSPSL phase inverter. (a) Its equivalent circuit model. The comparison between the simulated results and calculated curves at 1.5 GHz for (b) magnitude of S_{11} and (c) 180°−S_{21} are shown.

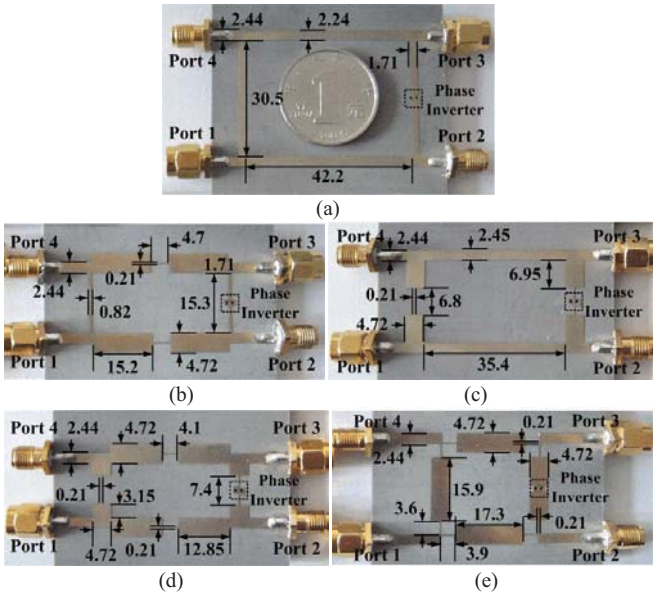

Fig. 10. Photos of the fabricated dual-band rat-race coupler prototypes with arbitrary power divisions. (a) UI schematic. (b) SI1 schematic. (c) SI2 schematic. (d) LHLH schematic. (e) HLHL schematic. The unit of dimensions is mm.

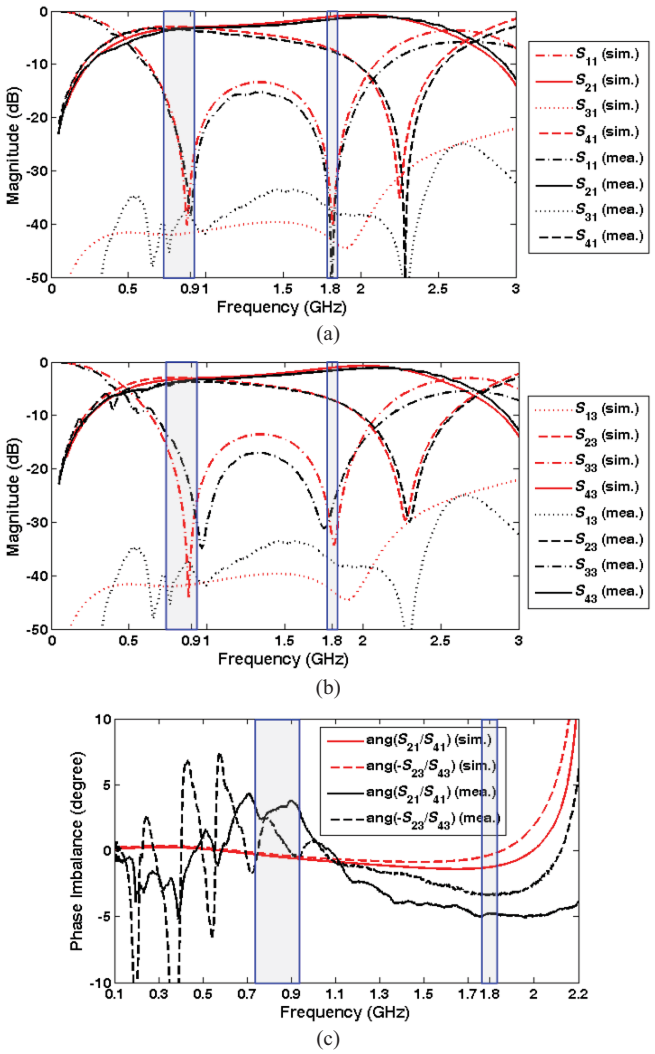

Fig. 11. Measured and simulated S-parameters of the uniform-impedance dual-band rat-race coupler prototype with arbitrary power divisions. (a) In-phase magnitudes. (b) Out-of-phase magnitudes. (c) Phase imbalance.

the used phase inverter is not significant for low operating frequencies, which will be demonstrated by the simulated and measured results of the rat-race couplers shown in the following parts.

B. Uniform-Impedance Dual-Band Rat-Race Coupler Prototype With Arbitrary Power Divisions

A rat-race coupler of the uniform-impedance schematic is designed, firstly, for 0.9 and 1.8 GHz ($n = 2$) to validate our method. The specific power divisions at the first and second bands are $R_{p1} = 1.0$ (0 dB) and $R_{p2} = 2.0$ (6 dB), respectively. The synthesized parameters are given in Table I. Its circumference is 245° at 0.9 GHz, which is only 45% of that of the conventional 540° counterpart, and its normalized area is reduced by about 80%.

As shown in Fig. 10(a), the prototype is fabricated on the same F4B substrate as the DSPSL phase inverter. The synthesized characteristic admittances and electrical lengths are utilized as the initial geometric parameters. Because of the effects of width steps, the DSPSL phase inverter and three-port conjunctions are not considered in the synthesis and the critical dimensions of the prototype are further optimized with its in-phase S-parameters by using Ansoft HFSS. Its measured S-parameters are plotted in Fig. 11, with the simulated ones also provided for comparison.

Some explanations for this coupler prototype are given as follows.

1) Its measured in-phase performance satisfies the corresponding specifications and agrees well with the simulated ones, and good isolation and phase balance are observed.
2) There is a slight deviation between the simulated and measured out-of-phase results, which is caused by the nonideal performance of the DSPSL phase inverter and its fabrication tolerance. This can be, however, eliminated by carefully optimizing of both the in-phase and out-of-phase performances.
3) The ripples of S_{23} at low frequencies are caused by the nonideal performance of the phase inverter. The electrical connection between the plated through holes and strips is not so reliable.

A transmission zero for S_{41} and S_{23} is found above the second operating band, which is important to tune the

TABLE II
COMPARISON OF THE MEASURED RESULTS OF THE DUAL-BAND RAT-RACE COUPLER PROTOTYPES WITH ARBITRARY POWER DIVISIONS BETWEEN DIFFERENT SCHEMATICS

@ 0.9 and 1.8 GHz	UI	SI1	SI2	LHLH	HLHL
$\|S_{11}\|$ in-phase	**–37.8 –39.9**	**–24.9 –35.0**	**–26.0 –29.1**	**–22.4 –30.0**	**–31.9 –10.0**
$\|S_{21}\|$ in-phase	–3.3 –1.6	–3.6 –1.8	–3.5 –1.7	–3.7 –1.8	–3.6 –3.4
$\|S_{41}\|$ in-phase	–3.6 –7.5	–3.9 –7.7	–3.7 –7.6	–4.1 –7.9	–3.9 –9.1
$\|S_{33}\|$ out-of-phase	–25.0 –27.8	–20.0 –25.4	–25.4 –46.5	–23.1 –36.5	–23.7 –11.7
$\|S_{23}\|$ out-of-phase	–3.7 –7.1	–3.9 –7.3	–3.8 –7.1	–3.9 –7.3	–3.7 –7.3
$\|S_{43}\|$ out-of-phase	–3.5 –1.6	–3.7 –1.7	–3.7 –1.7	–3.9 –1.8	–3.6 –3.5
$\|S_{31}\|$ isolation	**–38.6 –37.3**	**–35.5 –36.2**	**–43.8 –44.6**	**–44.4 –46.6**	**–28.6 –28.5**
$\|S_{21}/S_{41}\|$ in-phase	**0.3 5.9**	**0.3 5.9**	**0.2 5.9**	**0.4 6.1**	**0.3 5.7**
$\|S_{43}/S_{23}\|$ out-of-phase	0.2 5.5	0.2 5.6	0.1 5.4	0.0 5.5	0.1 3.8
$\angle S_{21} - \angle S_{41}$ in-phase	**3.8 –4.7**	**4.6 –4.0**	**3.2 –2.6**	**3.6 –1.8**	**1.9 –5.3**
$\angle S_{23} - \angle S_{43}$ out-of-phase	**179.7 176.7**	**178.8 176.9**	**180.3 180.3**	**178.5 181.1**	**179.7 182.6**
Fractional bandwidth	**22% 3.9%**	**9.0% 5.8%**	**13% 5.2%**	**9.2% 6.1%**	**35% /**

The magnitudes and amplitude imbalances are in dB. The phase imbalances are in degrees. These values are also applied to Table IV.

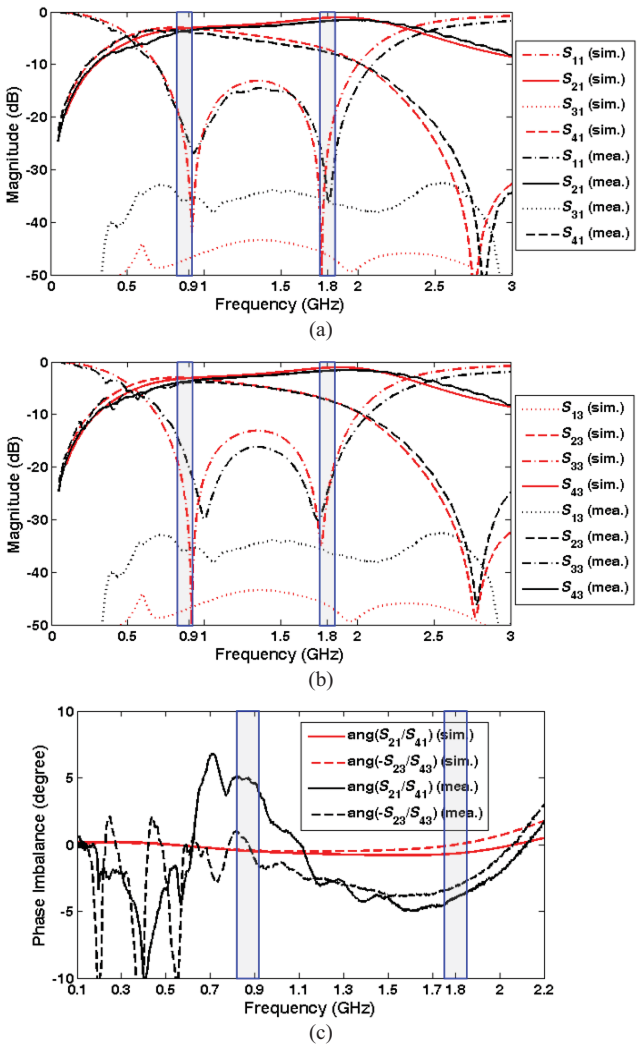

Fig. 12. Measured and simulated S-parameters of the SI1 dual-band rat-race coupler prototype. (a) In-phase magnitudes. (b) Out-of-phase magnitudes. (c) Phase imbalance.

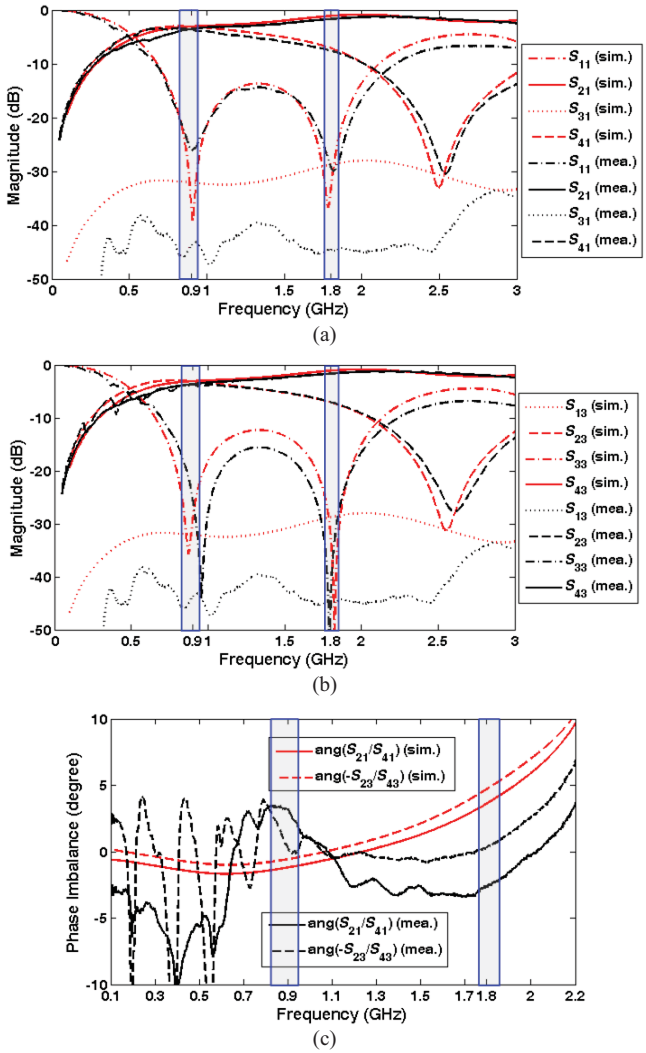

Fig. 13. Measured and simulated S-parameters of the SI2 dual-band rat-race coupler prototype. (a) In-phase magnitudes. (b) Out-of-phase magnitudes. (c) Phase imbalance.

power division ratio of the second band. Its location f_{z41} is determined by

$$\frac{S_{41}}{S_{21}} = \frac{-S_{23}}{S_{43}} = \frac{a-d}{2} = \frac{Y_{21}^{B}}{Y_{21}^{A}} = 0. \tag{20}$$

In other words, the transmission zeros of S_{41} and S_{23} arise at the zeros of Y_{21}^{B} and the poles of Y_{21}^{A}. For the uniform-impedance rat-race coupler, the frequency of the first transmission zero f_{z41} is calculated by

$$f_{z41} = \frac{\pi}{\theta_1} f_1. \tag{21}$$

The measured results of concern for the uniform-impedance dual-band rat-race coupler prototype are summarized in Table II. The fractional bandwidths in this paper are measured under all of the following conditions: $|S_{11}| \leq -15$ dB, $|S_{31}| \leq -20$ dB, -0.5 dB$\leq$ $|S_{21}/S_{41}| - R_{pi} \leq 0.5$ dB, $|\angle S_{21} - \angle S_{41}| \leq 5°$, and $|\angle S_{23} - \angle S_{43} - 180°| \leq 5°$, where $i = 1$ and 2. The measured operating bands are marked with blue panes in the plotted results. Due to the utilization of a phase inverter, the bandwidths limited by isolation and phase imbalances are much wider than the others. Then, the bandwidths are mainly determined by the power-division conditions. Because the power-division ratio R_{p1} at 0.9 GHz is 6 dB smaller than the ratio R_{p2} at 1.8 GHz, the variation of $|S_{21}/S_{41}|$ is relatively large. This leads to the two fractional bandwidths of 22% and 3.9%, which are smaller than that of a single-band rat-race coupler with a phase inverter.

C. Stepped-Impedance Dual-Band Rat-Race Coupler Prototypes With Arbitrary Power Divisions

As shown in Fig. 10(b)–(e), four stepped-impedance DSPSL rat-race coupler prototypes, including SI1, SI2, LHLH, and HLHL schematics, are designed with the same specifications and substrate as the uniform-impedance one. Their circumferences are equal to 174°, 199°, 159°, and 156° at 0.9 GHz. In comparison with the conventional 540° rat-race coupler, the largest area reduction of 92% is achieved with the HLHL case. But this schematic is not preferred here, which will be explained later. Their simulated and measured S-parameters

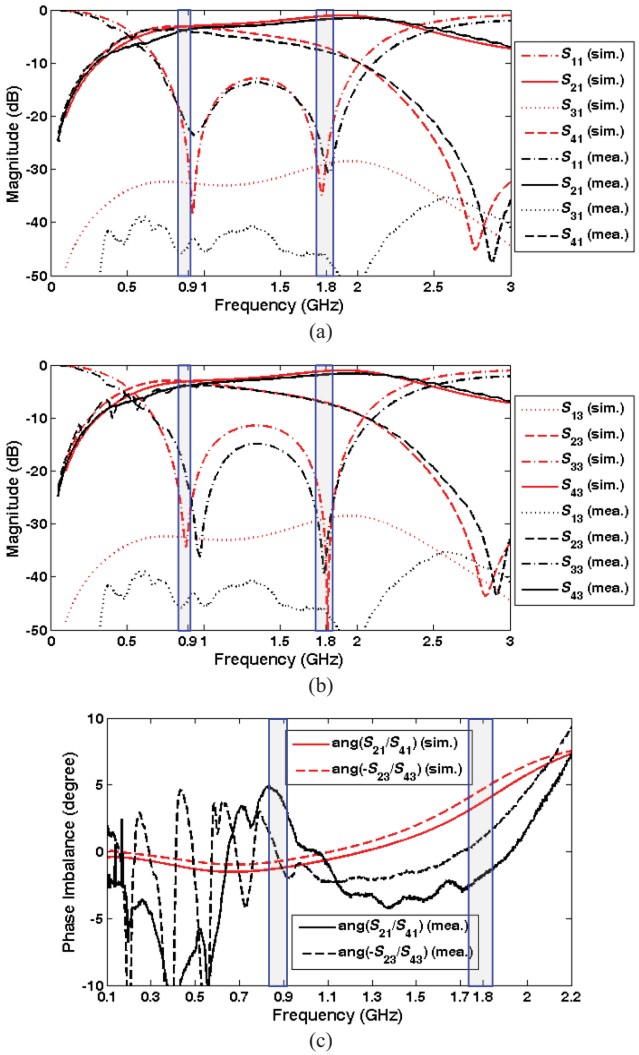

Fig. 14. Measured and simulated S-parameters of the LHLH dual-band rat-race coupler prototype are shown. (a) In-phase magnitudes. (b) Out-of-phase magnitudes. (c) Phase imbalance.

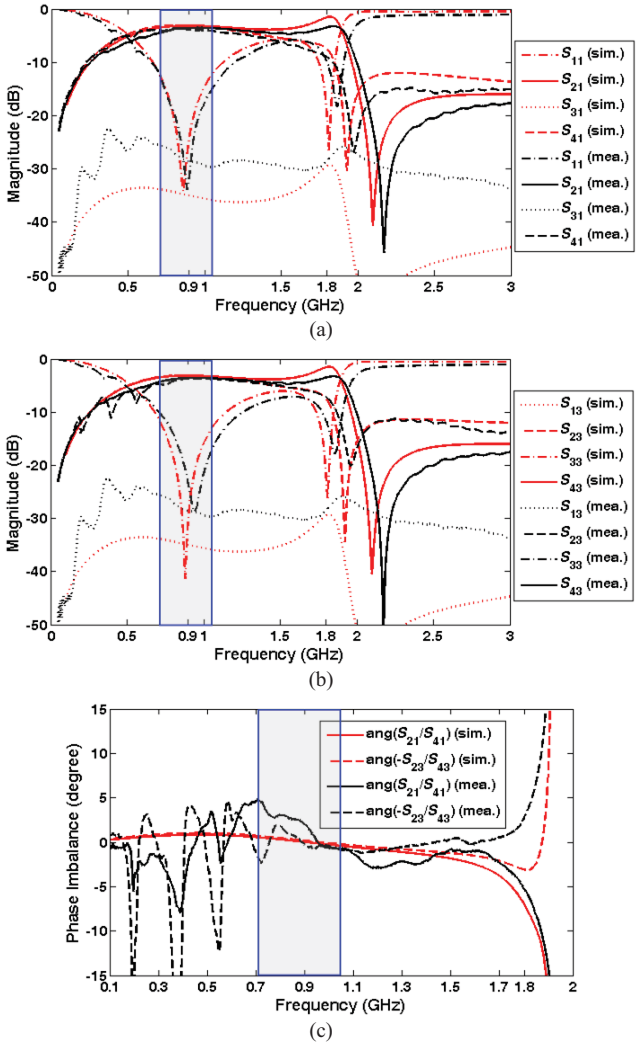

Fig. 15. Measured and simulated S-parameters of the HLHL dual-band rat-race coupler prototype are shown. (a) In-phase magnitudes. (b) Out-of-phase magnitudes. (c) Phase imbalance.

are plotted in Figs. 12–15, and our concerned dual-band measured results of them are summarized in Table II.

It is observed that the in-phase and out-of-phase insertion losses, i.e., $10\cdot\log_{10}(|S_{21}|^2 + |S_{41}|^2)$ and $10\cdot\log_{10}(|S_{23}|^2 + |S_{43}|^2)$, of the stepped-impedance rat-race couplers are larger than those of the uniform-impedance counterpart. This is caused by the used high-impedance transmission lines with a very narrow strip width and a relatively high attenuation constant.

For the SI1, SI2, and LHLH schematics, the fractional bandwidths of the first and the second operating bands are reduced and increased, respectively, because the low–high–low stepped-impedance sections are utilized. The LHLH rat-race coupler prototype provides the desired performances with an area reduction of 91%, in comparison with its conventional 540° counterpart.

By using the high–low–high sections, the bandwidth of the first band of the HLHL rat-race coupler is wider than that of its uniform-impedance counterpart. However, no suitable bandwidth is measured around 1.8 GHz. And it is noted that the transmission zeros of S_{21}, S_{41}, S_{23}, and S_{43} are all located near 1.8 GHz, which results in a significant increase of the corresponding insertion losses. The performance of the HLHL rat-race coupler around 1.8 GHz is also very sensitive to the fabrication tolerance. Therefore, the HLHL schematic is not suitable for this set of design specifications.

D. Validation for Different Design Specifications

As shown in Fig. 16, another two stepped-impedance rat-race coupler prototypes are developed under two different sets of design specifications, which are given by the following.

Case 2: $f_1 = 0.9$ GHz, $f_2 = 1.35$ GHz, $R_{p1} = 1.41$ (3 dB), and $R_{p2} = 2.0$ (6 dB).

Case 3: $f_1 = 0.9$ GHz, $f_2 = 2.25$ GHz, $R_{p1} = 0.71$ (–3 dB), and $R_{p2} = 1.41$ (3 dB).

Their synthesized critical geometric parameters are given in Table III. The information of the LHLH prototype in Fig. 10(d) is also listed as Case 1 for comparison. It is found that different stepped-impedance schematics, such as LHLH, HLLH, and LHHL cases, are preferred for different

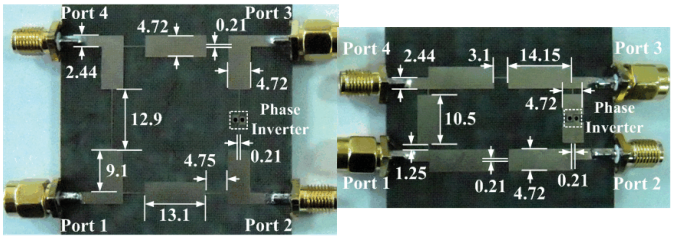

Fig. 16. Photos of the fabricated dual-band rat-race coupler prototypes of (a) Case 2 and (b) Case 3. The unit of dimensions is mm.

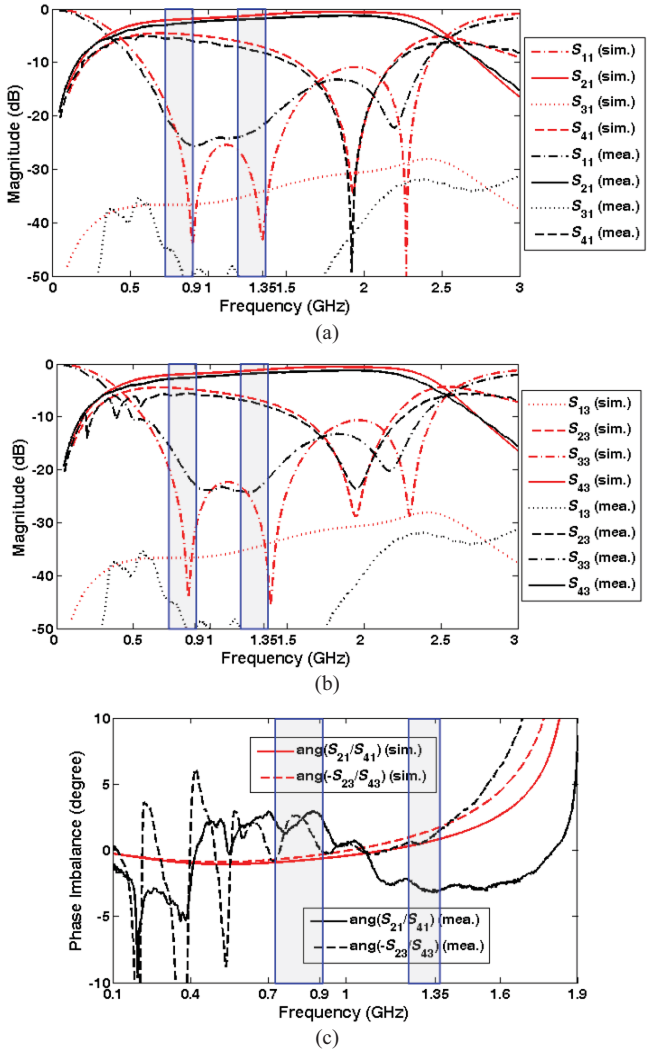

Fig. 17. Measured and simulated S-parameters of the HLLH dual-band rat-race coupler prototype for the design specification of Case 2. (a) In-phase magnitudes. (b) Out-of-phase magnitudes. (c) Phase imbalance.

sets of design specifications. A circumference reduction of 65%–70% can always be achieved by using our proposed dual-band design method, in comparison with the conventional 540° counterpart. Further, the circumferences of stepped-impedance prototypes are 21%–36% smaller than those of the uniform-impedance ones.

The simulated and measured S-parameters are plotted in Figs. 17 and 18. The measured results of concern in Table IV

TABLE III

COMPARISON OF THE SYNTHESIZED PARAMETERS BETWEEN THE DUAL-BAND RAT-RACE COUPLERS WITH ARBITRARY POWER DIVISIONS UNDER DIFFERENT DESIGN SPECIFICATIONS

	Case 1	Case 2	Case 3
Y_{1A}^{-1}	30.0	210	30.0
θ_{1A}	55.8	16.5	53.0
Y_{1B}^{-1}	210	30.0	210
θ_{1B}	6.07	23.4	4.25
Y_{2A}^{-1}	30.0	30.0	210
θ_{2A}	7.29	35.3	4.75
Y_{2B}^{-1}	210	210	30.0
θ_{2B}	10.5	18.5	19.8
ϕ	159	187	164
a_1	0.65	0.64	0.79
a_2	0.30	0.35	0.30

The design specifications of Case 1 is given by $f_1 = 0.9$ GHz, $f_2 = 1.8$ GHz, $R_{p1} = 1$ (0 dB), and $R_{p2} = 2.0$ (6 dB).

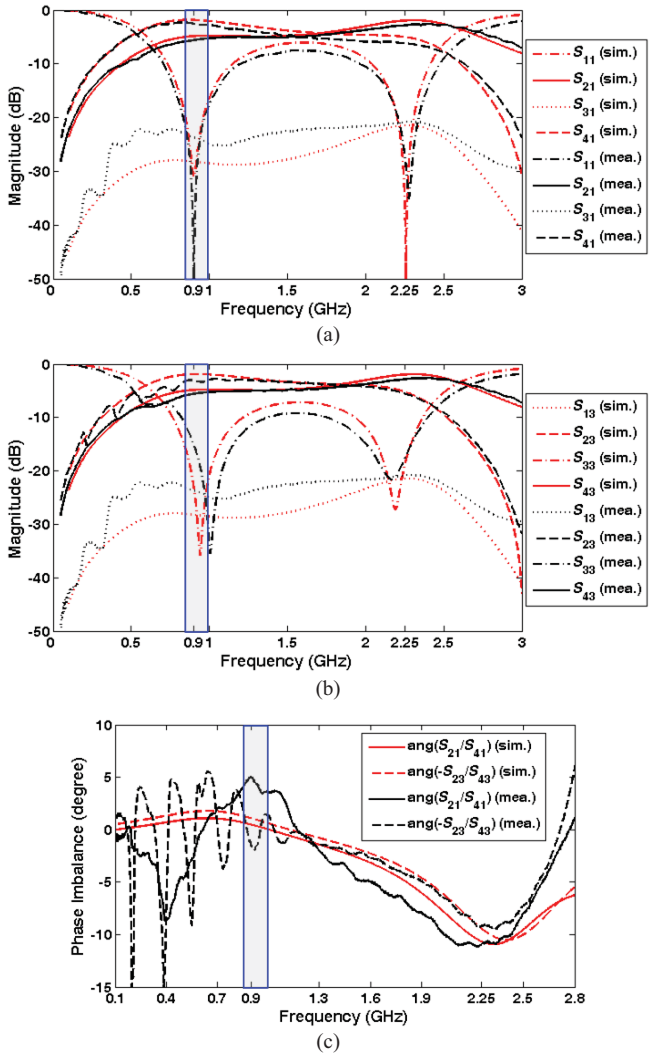

Fig. 18. Measured and simulated S-parameters of the LHHL dual-band rat-race coupler prototype for the design specification of Case 3. (a) In-phase magnitudes. (b) Out-of-phase magnitudes. (c) Phase imbalance.

show that these prototypes can provide good performances to satisfy their design specifications, except for the relatively large phase imbalances at the second band of Case 3, because

TABLE IV
COMPARISON OF THE MEASURED RESULTS BETWEEN THE DUAL-BAND RAT-RACE COUPLER PROTOTYPES WITH ARBITRARY POWER DIVISIONS UNDER DIFFERENT DESIGN SPECIFICATIONS

@ First and second band	Case 1	Case 2	Case 3
$\|S_{11}\|$ in-phase	**–22.4** **–30.0**	**–25.6** **–21.9**	**–63.9** **–27.1**
$\|S_{21}\|$ in-phase	–3.7 –1.8	–2.5 –1.8	–5.6 –2.9
$\|S_{41}\|$ in-phase	–4.1 –7.9	–6.0 –8.2	–2.6 –6.2
$\|S_{33}\|$ out-of-phase	–23.1 –36.5	–22.8 –22.6	–15.1 –17.7
$\|S_{23}\|$ out-of-phase	–3.9 –7.3	–5.7 –7.9	–3.1 –5.6
$\|S_{43}\|$ out-of-phase	–3.9 –1.8	–2.6 –1.7	–5.6 –2.9
$\|S_{31}\|$ isolation	**–44.4** **–46.6**	**–51.0** **–53.0**	**–23.8** **–20.8**
$\|S_{21}/S_{41}\|$ in-phase	**0.4** **6.1**	**3.5** **6.4**	**–3.0** **3.3**
$\|S_{43}/S_{23}\|$ out-of-phase	0.0 5.5	3.1 6.2	–2.5 2.7
$\angle S_{21} - \angle S_{41}$ in-phase	**3.6** **–1.8**	**2.7** **–3.0**	**5.0** **–11.0**
$\angle S_{23} - \angle S_{43}$ out-of-phase	**178.5** **181.1**	**180.2** **181.3**	**178.5** **170.8**
Fractional bandwidth	**9.2%** **6.1%**	**20%** **9.0%**	**16%** **/**

The design specifications of Case 1 is given by $f_1 = 0.9$ GHz, $f_2 = 1.8$ GHz, $R_{p1} = 1$ (0 dB), and $R_{p2} = 2.0$ (6 dB).

of the nonideal influence of the phase inverter, especially on the high-frequency operating band. By further optimizing the geometric parameters of the DSPSL phase inverter to shorten the equivalent length of additional transmission line and using more reliable processes for plated through holes, a high operating frequency will also be achieved. We would like to say that the flexible applications of our proposed method have been verified for the design of miniaturized dual-band rat-race coupler with arbitrary power divisions.

Evidently, our designed dual-band rat-race couplers with arbitrary power divisions are more compact than those proposed in [20] and [21], because the design of the arms here are no more started from the conventional 90° and 270° sections and a phase inverter is introduced to replace a 180° section. In addition, all the operating bands of our developed coupler prototypes are the first-order ones (each operating band only have one reflection zero), while those in [20] and [21] are the second-order ones (each operating band may have two reflection zeros). However, the fractional bandwidths of our coupler prototypes are still comparable to those in [20], because of the successful utilization of phase inverter.

VII. CONCLUSION

In this paper, a new type of miniaturized dual-band rat-race coupler with arbitrary power divisions was proposed and studied in detail. Some generalized equations were derived for the synthesis of dual-band rat-race coupler with a phase inverter. Its arms were no longer limited to simulate 90° sections and the stepped-impedance technique was applied to them. The relationships between the geometries and design specifications were characterized. By using the maximum allowable impedance ratio for all four arms, our proposed rat-race couplers will have the most compact configuration. The circumferences of the dual-band coupler with arbitrary power divisions were significantly reduced by 65%–70%, in comparison with the conventional 540° counterpart. Several DSPSL prototypes have been developed to validate our design method, with good performances demonstrated numerically and experimentally.

REFERENCES

[1] C. Y. Pon, "Hybrid-ring directional coupler for arbitrary power division," *IEEE Trans. Microw. Theory Tech.*, vol. 9, no. 6, pp. 529–535, Nov. 1961.

[2] A. K. Agrawal and G. F. Mikucki, "A printed-circuit hybrid-ring directional coupler for arbitrary power divisions," *IEEE Trans. Microw. Theory Tech.*, vol. 34, no. 12, pp. 1401–1407, Dec. 1986.

[3] Y.-C. Chiou, J.-S. Wu, and J.-T. Kuo, "Periodic stepped-impedance rat race coupler with arbitrary power division," in *Asia-Pacific Microw. Conf. Dig.*, Dec. 2006, pp. 663–666.

[4] T.-Q. Wang and K. Wu, "Size-reduction and band-broadening design technique of uniplanar hybrid ring coupler using phase inverter for M(H)MIC's," *IEEE Trans. Microw. Theory Tech.*, vol. 47, no. 2, pp. 198–206, Feb. 1999.

[5] C.-Y. Chang and C.-C. Yang, "A novel broad-band Chebyshev-response rat-race ring coupler," *IEEE Trans. Microw. Theory Tech.*, vol. 47, no. 4, pp. 455–462, Apr. 1999.

[6] K.-K. M. Cheng and F.-L. Wong, "A novel rat race coupler design for dual-band applications," *IEEE Microw. Wireless Compon. Lett.*, vol. 15, no. 8, pp. 521–523, Aug. 2005.

[7] K.-K. M. Cheng and F.-L. Wong, "Dual-band rat-race coupler design using tri-section branch-line," *Electron. Lett.*, vol. 43, no. 6, pp. 41–42, Mar. 2007.

[8] H. Zhang and K.-J. Chen, "Design of dual-band rat-race couplers," *IET Microw. Antennas Propag.*, vol. 3, no. 3, pp. 514–521, Apr. 2009.

[9] C.-L. Hsu, C.-W. Chang, and J.-T. Kuo, "Design of dual-band microstrip rat race coupler with circuit miniaturization," in *IEEE MTT-S Int. Microw. Symp. Dig.*, Honolulu, HI, Jun. 2007, pp. 177–180.

[10] G.-Q. Liu, L.-S. Wu, and W.-Y. Yin, "Miniaturised dual-band rat-race coupler based on double-sided parallel stripline," *Electron. Lett.*, vol. 47, no. 14, pp. 800–802, Jul. 2011.

[11] L. Chiu and Q. Xue, "Investigation of a wideband 90° hybrid coupler with an arbitrary coupling level," *IEEE Trans. Microw. Theory Tech.*, vol. 58, no. 4, pp. 1022–1029, Apr. 2010.

[12] K.-S. Chin, K.-M. Lin, Y.-H. Wei, T.-H. Tseng, and Y.-J. Yang, "Compact dual-band branch-line and rat-race couplers with stepped-impedance-stub lines," *IEEE Trans. Microw. Theory Tech.*, vol. 58, no. 5, pp. 1213–1221, May 2010.

[13] Y.-C. Chiou, J.-T. Kuo, and C.-H. Chan, "New miniaturized dual-band rat-race coupler with microwave C-sections," in *IEEE MTT-S Int. Microw. Symp. Dig.*, Boston, MA, Jun. 2009, pp. 701–704.

[14] Y.-C. Liu, W.-H. Chen, and Z.-H. Feng, "Compact dual-band branch-line and rat-race couplers with stepped coupled-line," in *China-Jpn. Joint Microw. Conf. Dig.*, Hangzhou, China, Apr. 2011, pp. 1–4.

[15] I.-H. Lin, M. DeVincentis, C. Caloz, and T. Itoh, "Arbitrary dual-band components using composite right/left-handed transmission lines," *IEEE Trans. Microw. Theory Tech.*, vol. 52, no. 4, pp. 1142–1149, Apr. 2004.

[16] P.-L. Chi, C.-J. Lee, and T. Itoh, "A compact dual-mand metamaterial-based rat-race coupler for a MIMO system application," in *IEEE MTT-S Int. Microw. Symp. Dig.*, Atlanta, GA, Jun. 2008, pp. 667–670.

[17] T.-M. Shen, C.-R. Chen, T.-Y. Huang, and R.-B. Wu, "Dual-band rat-race coupler design in multilayer LTCC," in *Asia-Pacific Microw. Conf. Dig.*, Yokohama, Japan, Dec. 2010, pp. 798–801.
[18] G. Siso, J. Bonache, and F. Martin, "Dual-band rat race hybrid coupler implemented through artificial lines based on complementary split ring resonators," in *IEEE MTT-S Int. Microw. Symp. Dig.*, Boston, MA, Jun. 2009, pp. 625–628.
[19] Y.-D. Dong and T. Itoh, "Application of composite right/left-handed half-mode substrate integrated waveguide to the design of a dual-band rat-race coupler," in *IEEE MTT-S Int. Microw. Symp. Dig.*, Anaheim, CA, May 2010, pp. 712–715.
[20] C.-L. Hsu, J.-T. Kuo, and C.-W. Chang, "Miniaturized dual-band hybrid couplers with arbitrary power division ratios," *IEEE Trans. Microw. Theory Tech.*, vol. 57, no. 1, pp. 149–156, Jan. 2009.
[21] C.-Y. Wu, Y.-C. Chiou, and J.-T. Kuo, "Dual-band rat-race coupler with arbitrary power divisions using microwave C-sections," in *Asia-Pacific Microw. Conf. Dig.*, Singapore, Dec. 2009, pp. 2108–2111.
[22] L.-S. Wu, J. Mao, and W.-Y. Yin, "Compact rat-race coupler with double-sided parallel-strip line (DSPSL) for dual-band arbitrary power divisions," in *Asia-Pacific Microw. Conf. Dig.*, Melbourne, Australia, Dec. 2011, pp. 880–883.

Lin-Sheng Wu (S'09–M'10) was born in 1981. He received the B.S. degree in electronic and information engineering and the M.S. and Ph.D. degrees in electromagnetic fields and microwave technologies from Shanghai Jiao Tong University (SJTU), Shanghai, China, in 2003, 2006, and 2010, respectively.

He was a Research Fellow with the Department of Electrical and Computer Engineering, National University of Singapore, Singapore, from August 2010 to November 2010. From 2010 to 2012, he was a Post-Doctoral Researcher with SJTU. He is currently a Lecturer with the Key Laboratory of Ministry of Education for Research of Design and Electromagnetic Compatibility of High Speed Electronic Systems, SJTU. His current research interests include novel techniques for microwave integration, passive components, and carbon nanoelectronics. He is the author or co-author of more than 50 technical papers.

Dr. Wu was a Session Co-Chair of Asia-Pacific Microwave Conference and the IEEE Electrical Design of Advanced Packaging and Systems Symposium in 2011. He is a reviewer of several international journals, including three IEEE TRANSACTIONS AND LETTERS.

Junfa Mao (M'92–SM'98–F'12) was born in 1965. He received the B.S. degree in radiation physics from the University of Science and Technology of National Defense, Hefei, China, in 1985, the M.S. degree in experimental nuclear physics from the Shanghai Institute of Nuclear Research, Shanghai, China, in 1988, and the Ph.D. degree in electronic engineering from Shanghai Jiao Tong University (SJTU), Shanghai, in 1992.

He has been a Faculty Member with SJTU since 1992, where he is currently a Chair Professor and the Executive Dean of the School of Electronic, Information and Electrical Engineering. He was a Visiting Scholar with the Chinese University of Hong Kong, Hong Kong, from 1994 to 1995, and a Post-Doctoral Researcher with the University of California, Berkeley, from 1995 to 1996. His current research interests include the interconnect and package problem of integrated circuits and systems, analysis, and design of microwave circuits. He has authored or co-authored more than 190 journal papers, including 70 IEEE journal papers, and 120 international conference papers.

Dr. Mao was a recipient of the National Natural Science Award of China in 2004, the National Technology Invention Award of China in 2008, and the Best Paper Award at the Symposium of APEMC in conjunction with the 19th International Symposium of Zurich EMC in 2008. He is a Chief Scientist of the National Basic Research Program 973 Program of China, a Project Leader of the National Science Foundation for Creative Research Groups of China, a Cheung Kong Scholar of the Ministry of Education, China, and an Associate Director of the Microwave Society of China Institute of Electronics. He was the Chair of the IEEE Shanghai Section from 2007 to 2009 and the Chair of IEEE MTT Shanghai Chapter from 2009 to 2011.

Wen-Yan Yin (M'99–SM'01) received the M.Sc. degree in electromagnetic fields and microwave techniques from Xidian University, Xi'an, China, in 1989, and the Ph.D. degree in electrical engineering from Xi'an Jiao Tong University, Xi'an, in 1994.

He was an Associate Professor with the Department of Electronic Engineering, Northwestern Polytechnic University, Xi'an, from 1993 to 1996. From 1996 to 1998, he was a Research Fellow with the Department of Electrical Engineering, Duisburg University, Duisburg, Germany, under a grant from the Alexander von Humboldt-Stiftung, Bonn, Germany. In 1998, he joined the Monolithic Microwave Integrated Circuit Modeling and Package Laboratory, Department of Electrical Engineering, National University of Singapore, Singapore, as a Research Fellow, where he joined the Temasek Laboratories as a Research Scientist and the Project Leader of high-power microwave and ultrawideband electromagnetic compatibility/EMI in 2002. Since April 2005, he has been a Professor of electromagnetic fields and microwave techniques with the School of Electronic Information and Electrical Engineering, Shanghai Jiao Tong University, Shanghai, China, where he is also the Director and an Adjunct Ph.D. He is a Candidate Supervisor with the Center for Microwave and RF Technologies. Since 2009, he has been with the Center for Optical and Electromagnetic Research, National State Key Laboratory of Modern Optical Instrumentation, Zhejiang University, Hangzhou, China, as a "Qiu Shi" Chair Professor. He has authored or co-authored more than 190 published international journal articles, including more than 70 IEEE papers, one international book, and 17 book chapters, including the chapter "Complex Media" in the *Encyclopedia of RF and Microwave Engineering* (John Wiley & Sons, 2005). His current research interests include passive and active RF and millimeter-wave devices and circuit modeling, ultra wideband interconnects and signal integrity, nanoelectronics, electromagnetic compatibility, electromagnetic protection of communication platforms, and computational multiphysics and its applications.

Dr. Yin was a recipient of the Science and Technology Promotion Award of the First Class from the local Shanghai Government of China in 2005, the National Technology Invention Award of the Second Class from the Chinese Government in 2008, and the Best Paper Award from the 2008 Asia-Pacific Symposium on Electromagnetic Compatibility and the 19th International Zurich Symposium in Singapore. He has been a Guest Editor of the IEEE TRANSACTIONS ON COMPONENTS, PACKAGING AND MANUFACTURING TECHNOLOGY since 2011 and an Associate Editor of the *International Journal of Electronic Networks, Devices and Fields* since 2011. He is an Editorial Board Member of the *International Journal of RF and Microwave CAE*, JEMWA, and *Progress in Electromagnetics Research*. He is a reviewer of many international journals, including eight IEEE TRANSACTIONS AND LETTERS. He was the Technical Chair of EDAPS in 2006, the General Co-Chair of the IEEE Electrical Design of Advanced Packaging and Systems Symposium (EDAPS) in 2011, technically sponsored by IEEE CPMT Committee, and the IEEE EMC Society Distinguished Lecturer from 2011 to 2012.